Vol. 46, No. 1 (2024) 116-125, DOI: 10.24874/ti.1544.09.23.11

Tribology in Industry

www.tribology.rs

RESEARCH

Micro-Scale Abrasive Wear Resistance of a Nanoceramic Sealant Applied on Galvanized Low Carbon Steel

Anael P. Krelling[a,*], Jefferson L. Jeronimo[a], Ivandro Bonetti[a], Gabriela Rabethge[a], Heitor F. Pensky[a], Raíssa R.S. Bibow[a], Bruna F. Zappelino[b], Julio C.G. Milan[c], Cesar E. da Costa[c]

[a]*Instituto Federal de Santa Catarina – IFSC, Joinville, Brazil,*
[b]*UniSENAI, Joinville, Brazil,*
[c]*Universidade do Estado de Santa Catarina – UDESC, Joinville, Brazil.*

Keywords:

Surface Engineering
Adhesion
Abrasive Wear
Tribology
Corrosion

* Corresponding author:

Anael P. Krelling
E-mail: anael.krelling@ifsc.edu.br

Received: 11 September 2023
Revised: 14 October 2023
Accepted: 2 November 2023

A B S T R A C T

The idea for this work came from a market need to obtain coatings or sealants that would extend the useful life of metallic materials in applications that involve exposure to corrosive environments. The main objective of the nanoceramic sealant studied in this work is to extend the life of metallic fasteners. To evaluate the performance of the sealant from other perspectives, microstructural analysis, adhesion test, micro-scale abrasive wear tests and corrosion test were carried out. These tests were performed on samples coated only with white zinc, which is commonly used in the fastener industry, and on samples coated with white zinc followed by application of the nanoceramic sealant. The application of the nanoceramic sealant contributed to the improvement of corrosion resistance and reduction of the corrosion rate. The corrosion rate of the sample coated with the sealant reduced by 62.2% when compared to the sample that only went through the white zinc coating process. The coating showed low adhesion to the substrate with the presence of severe delamination and microcracks. This feature contributed to the low wear resistance presented by the coating under the conditions studied in this work. Less attention, compared to studies involving corrosion resistance, has been given to wear resistance in the fastener industry. The results obtained in this paper show that the study of tribological behavior is an important factor in increasing the efficiency of fasteners applied in harsh environments.

© 2024 Published by Faculty of Engineering

1. INTRODUCTION

Due to industrial development, there is a need to use more sophisticated and/or miniaturized mechanisms. Therefore, the investigation of processes to improve surface properties is so important in order to achieve optimal conditions in industrial applications such as tribological performance and corrosion resistance [1]. There are a number of techniques to improve corrosion resistance of metal-based components such as coating techniques, anodic/cathodic

protection, use of inhibitors and so on [2]. Steels, zinc-coated steels or aluminum alloys used in many fields such as construction, transportation, industries and others require surface protection to prevent environmental degradation [3]. In fasteners industries, which is the focus of this paper, it is common to apply a zinc coating (conversion coating) to protect the carbon steel of the substrate from corrosion [4]. After the formation of the zinc coating, some organic coating can be applied in order to achieve an effective protection against corrosion [5,6].

Owing to the miniaturization of parts and systems, there was a need to find a test capable of obtaining information from the most superficial regions of these materials [7]. The micro-scale abrasive wear test (ball-cratering) is a well-known technique to determine tribological properties of surfaces. In this test, a ball is rotated against a specimen in the presence of an abrasive slurry [8,9]. The micro-abrasive wear test was developed in 1996 for the tribological evaluation of coated systems [10]. Industrially it is used to evaluate the coating thickness of specimens [11]. This test is considered fast, cheap, easy to use, and can be performed on small samples [12,13]. Some parameters such as wear rate (Q) and wear coefficient (k) can be used to differentiate abrasive wear and micro-scale abrasive wear. In abrasive wear, wear coefficients up to 100,000 times greater than those obtained for micro-scale abrasive wear are observed. In addition to the rate and wear coefficient, the difference between abrasive and micro-scale abrasive wear can be expressed in terms of the size of the abrasive particles. In micro-abrasive wear tests, abrasive particles of around 5 μm or smaller are commonly used [14–16]. The equipment used to carry out micro-scale abrasive wear tests can have two different configurations: I) fixed-ball and II) free-ball. In the first case the ball is fixed between two coaxial axes and the force is applied by a "dead weight" system through a lever. In the second case, the ball rests on an axis and the applied force are the weight of the ball [7,17,18]. In the micro-scale abrasive wear test the wear coefficient is a function of the wear crater diameter (b), the radius of the ball (R), the sliding distance (S) and the normal applied load (N) according to the formula (1):

$$k = \frac{\pi b^4}{64RSN} \text{ for } b \ll R \quad (1)$$

Currently, in many applications in the fastener industry, there is an interest in improving the corrosion resistance of manufactured elements. Therefore, the application of coatings is increasingly used. Less attention, however, has been given to the wear resistance of elements manufactured by these industries. Thus, the aim of this work is to investigate the micro-scale abrasive wear behavior, the corrosion resistance and the microstructure characteristics of a nanoceramic sealant applied over low-carbon galvanized steel specimens commonly used in the fasteners industry.

2. EXPERIMENTAL

2.1 Materials and coating

Samples, 6 mm thick, of AISI 1020 steel were cut from a 25 mm diameter bar. Both samples surface was ground and sanded with 320 grit sandpaper for surface standardization. Two surface condition were used, 15 samples were zinc coated (Zn-coating) and 15 underwent the zinc coating followed by the application of the nanoceramic sealant (Zn + nano-coating). For the application of the nanoceramic sealant, after the zinc coating, the samples were placed in a container and immersed for 40 s in a solution of water and nanoceramic sealant powder at room temperature. After immersion, the solution was removed from the container and the samples were centrifuged. Finally, the curing process was carried out in an electrical furnace at 180°C.

2.2 Coating characterization and corrosion resistance

X-Ray Diffraction Analysis (XRD) was used to determine the stoichiometry of the phases formed after the coating processes. Cu-Kα radiation was used, scanning angle (2θ) between 20° and 120° and scanning speed of 1°/min were the measurement parameters in the Shimadzu 6000 equipment using the bragg/bentano configuration.

The morphology and microstructure of the layers were evaluated using Scanning Electron Microscopy (SEM) in a Zeiss Gemini Supra 55VP microscope equipped with an Energy Dispersive Spectroscopy (EDS) probe.

The layer-substrate adhesion, in turn, was qualitatively evaluated using Rockwell C indentations according to the VDI 3198 standard (Figure 1). According to the standard, levels HF1, HF2, HF3 and HF4 are considered acceptable, as the coating must withstand small loads without microcracking or significant delamination. The HF5 and HF6 levels characterize unacceptable failures, that is, the coating has little adhesion in these configurations [19].

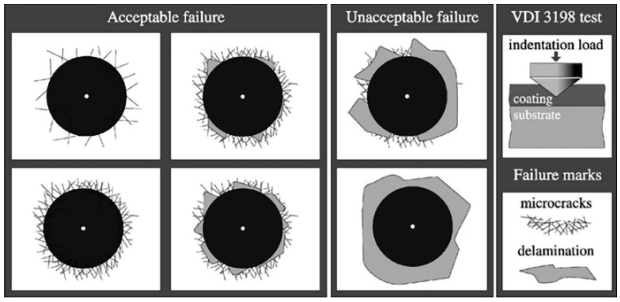

Fig. 1. The principle of the VDI 3198 indentation test.

For the potentiodynamic corrosion test, 3 samples of each surface condition were used. Corrosion behavior was evaluated after immersion of the samples for 1 hour in a solution with 3.5% by weight of NaCl and distilled water at room temperature, so that an almost stationary potential value was obtained. A three-electrode electrochemical cell connected to a Gamry 3000 potentiostat was used, using an Ag/AgCl reference electrode in a KCl-saturated medium, a platinum counter electrode and a working electrode (sample) with an exposed area of 1 cm^2. The sequence of tests carried out was programmed with an open circuit potential test with a test time of 3600 seconds and a sample period of 0.5 s and a potentiodynamic polarization test with an initial potential of -0.3 V, final potential of -0 .6V, acquisition rate of 1mV/s and sample period of 1 s.

2.3 Micro-scale abrasive wear tests

The micro-scale abrasive wear tests were performed with the Phoenix Tribology TE66-SLIM equipment. Before the beginning of each test cycle, the AISI 52100 steel ball was conditioned through mechanical agitation in a container with silica sand and distilled water for 5 minutes. After conditioning, the ball was ultrasonically cleaned in ethyl alcohol for 10 minutes. The Zn-coating and Zn + nano-coating samples were subjected to 3 tests under each load and abrasive slurry concentration condition. The diameters of the craters were optically measured in steps of 100 ball revolutions until 1200 revolutions, in order to identify the steady state regime. The tests were performed using an abrasive slurry mixture of SiO_2 particles (80% between 1-5 μm) by Sigma-Aldrich and distilled water, with a concentration of 0.244g/cm^3 and 0.733g/cm^3, which results in a volumetric concentration of 10% and 30%, respectively. The normal loads were 0.49 N and 0.98 N, and the rotary speed was 70 rpm.

3. RESULTS AND DISCUSSIONS

3.1 Microstructure characterization, evaluation of layer adhesion and corrosion resistance

As shown in Figure 2, it can be seen that XRD results for the Zn-coating sample shows the presence of metallic Zn and ferrite, coming from the substrate. On the other hand, the Zn + nano-coating sample features Zn, SiO_2 and Zn_2SiO_4 in the coating. Possibly, Zn_2SiO_4 was formed in the contact zone between the Zn layer and the nanoceramic sealant layer.

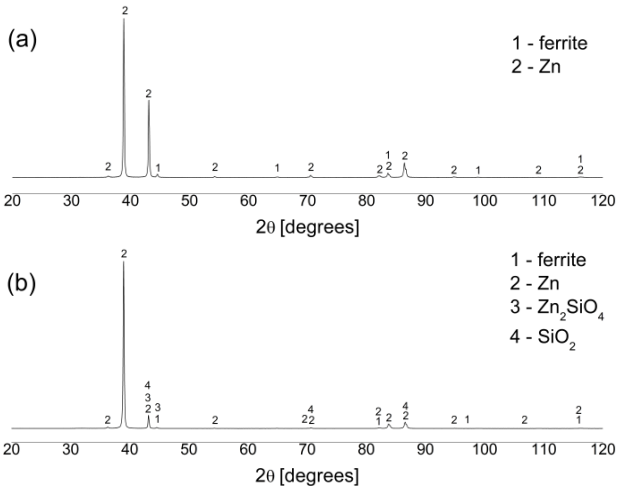

Fig. 2. XRD patterns of Zn-coating (a) and Zn + nano-coating (b) samples.

The cross-sections of the Zn-coating and Zn + nano-coating samples are presented in Figures 3 and 4, respectively.

In the Figure 3(a), two regions were identified in the Zn-coating cross-section: (1) Zn coating layer and (2) steel substrate. In Figure 3(b), the presence of Fe that appears in the image comes from the substrate of the sample. Due to the presence of Zn, observed in Figure 3(c), it can be considered that the Zn layer is uniform in terms of thickness and constant throughout the surface of the sample and has an average thickness of 7±0.7 μm.

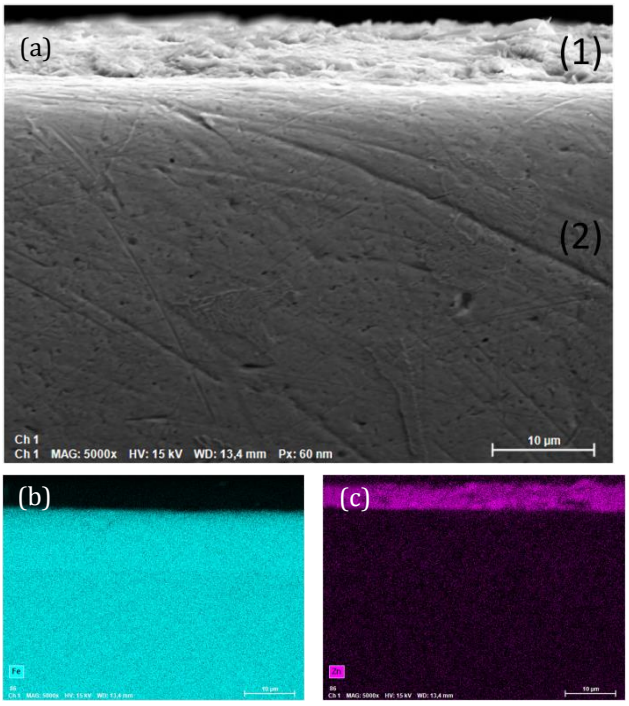

Fig. 3. (a) SEM image of the cross-section of the Zn-coating sample. (b)-(c) EDS mapping of Fe and Zn, respectively.

In Figure 4(a) 3 different regions were identified, which are: (1) nanoceramic sealant coating, (2) Zn layer from galvanization and (3) substrate. In addition to Fe (b) from the substrate and Zn (c), the presence of Si (d) and O (e) in the most superficial region of the sample is notable. In addition, there is formation of a compact and uniform layer over the entire surface of the sample, approximately 1µm thick, which allows us to conclude that the sealant layer is composed of SiO_2, as evidenced in the XRD results. It is common for nanoceramic sealants to have low coating layer thickness, usually in the order of nanometers, and good properties of wear resistance, hydrophobicity, chemical resistance, durability and UV protection [20,21].

The indentation on the Zn-coating sample, showed in Figure 5(a), did not present any anomaly. Adherence to steel was maintained at HF1 scale, which is considered an acceptable level of coating adhesion. Figure 5(b) is a magnification of the rectangle showed in Figure 5(a). On the other hand, the Zn + nano-coating indentation showed in Figure 5(c), can be classified as HF6 on the adhesion scale, which is not considered an acceptable level of coating adhesion, i.e., it failed the adhesion test within the established conditions and is prone to suffer significant micro-cracking or delamination as showed in Figure 5(d).

In order to evaluate the coating-substrate adhesion and its brittleness [22,23]. Rockwell C indentation tests were carried out on the Zn-coating and Zn + nano-coating samples.

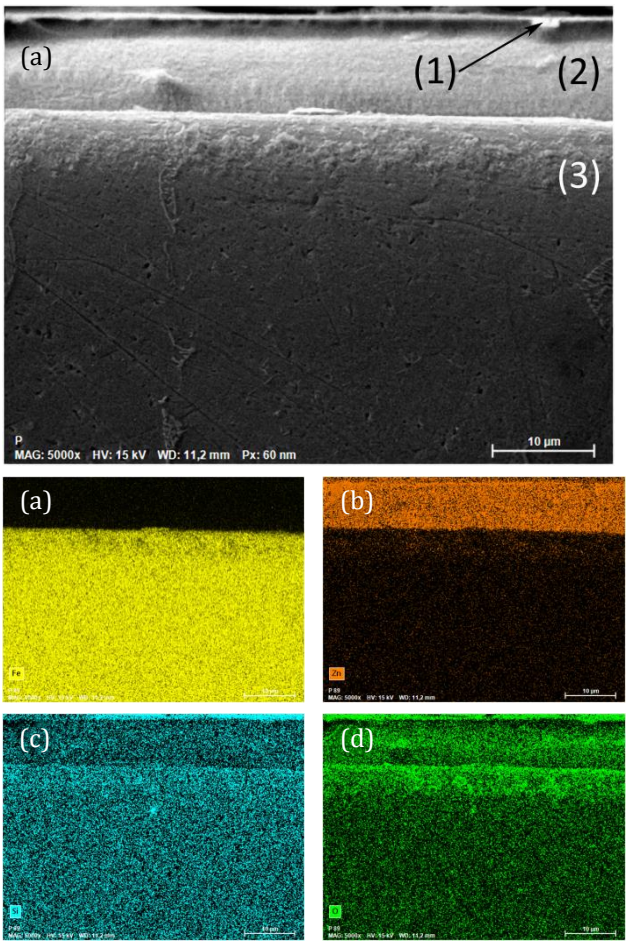

Fig. 4. (a) SEM image of the cross-section of the Zn + nano-coating sample. (b)-(e) EDS mapping of Fe, Zn, Si and O, respectively.

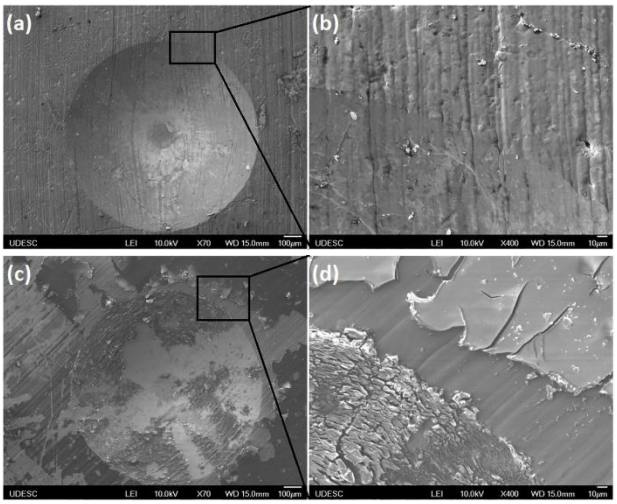

Fig. 5. SEM micrographs of the Rockwell C adhesion test on the Zn-coating (a) and Zn + nano-coating (c) samples. (b) and (d) are the magnified area indicated by the rectangle in (a) and (c), respectively.

The curves obtained through the potentiodynamic polarization test can be seen in Figure 6. The results were separated according to the surface treatment conditions for better visualization.

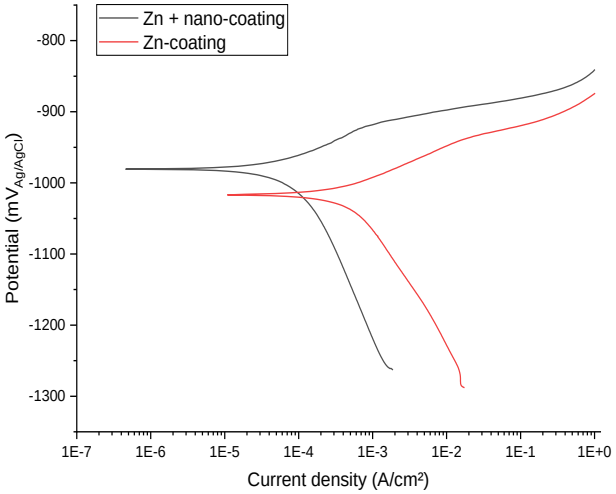

Fig. 6. Potentiodynamic polarization curves.

Analyzing the shape of the curve, it can be stated that all conditions tested remain in a state of degradation throughout the test. However, for both cases, at the beginning of the anodic polarization there is a reduction in the current density with an increase afterwards, this is probably due to the formation of a relatively dense passive film product of corrosion, which is unstable and is removed by the ions of the solution, increasing the current density. Xiao et al. studied the behavior of the Al-Zn coating on steel sheets in a corrosive environment that simulated the marine environment and observed the same behavior reported in the present study [24].

For the quantitative analysis of the results of the potentiodynamic polarization curve, the Tafel extrapolation method was used to obtain current density and corrosion potential values [25]. The corrosion potentials for the tested conditions were -971 mV to Zn + nano-coating and -995 mV to Zn-coating. Those values that were similar to those obtained for Zn in the study developed by Wang et al. [26]. It is important to point out that, regardless of the tested conditions, these measured potentials are characteristic values of reactions with greater activity. In addition, there is no statistical difference between the two conditions, as can be seen in Table 1.

Table 1. Potencial and corrosion rate adjusted by the Tafel method.

Condition	E_{corr} ($mV_{Ag/AgCl}$)	I_{corr} ($nAcm^2$)
Zn-coating	-995 ± 35.36	5.61E+02 ± 4.03E+01
Zn + nano-coating	-971 ± 14.14	2.12E+02 ± 1.67E+02

When the results are analyzed, a considerable reduction in the corrosion rate is observed. For the Zn-coating samples, the corrosion rate is 5.61E+02 nA/cm^2, while for the Zn + nano-coating samples, the corrosion rate is 2.12E+02 nA/cm^2, implying a reduction of 62.2%. Therefore, it is possible to state that the nanoceramic sealant contributed to the improvement of corrosion resistance and reduction of the corrosion rate.

3.2 Tribological behavior

In order to prove that the wear crater produced during the micro-scale abrasive wear tests reflected the counter-body geometry, i. e., a ball of 12.7 mm radius, the topographical analysis of the wear craters was carried out for each condition of the wear tests. In Figure 7 it is shown the Zn + nano-coating condition abraded with an abrasive slurry concentration of 0.244 g/cm^3 at an applied load of 0.98 N.

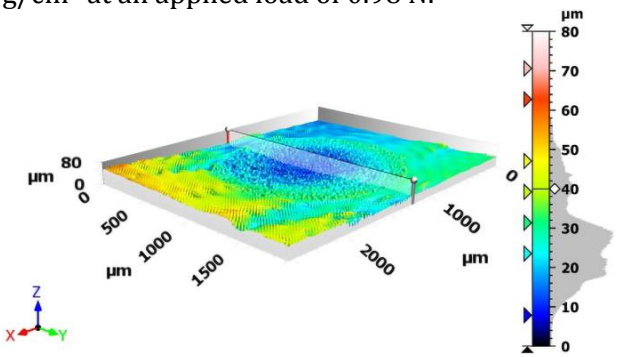

(a)

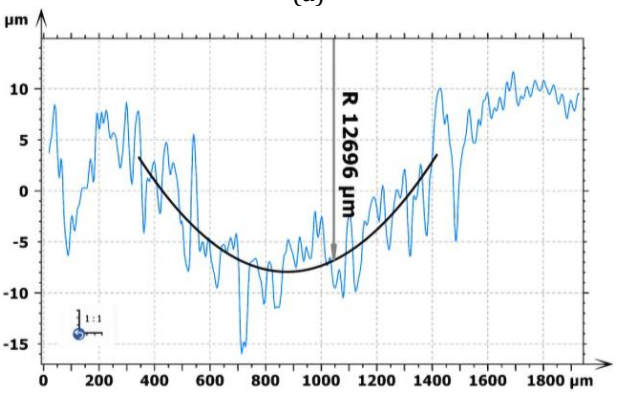

(b)

Fig. 7. Topographical analysis of the crater produced in a Zn + nano-coating specimen. (a) wear crater; (b) profile in the center of the crater.

As can be seen from Figure 7(b), the wear crater has a radius of 12.696 mm, thus validating the use of Formula (1) [27,28].

The identification of the steady state regime (SSR) of the micro-scale abrasive wear tests was determined by analyzing the graph of the wear coefficient (k) as a function of the sliding distance (S). In addition, the graph of wear volume (V) as a function of the sliding distance was used for the verification of obtaining the SSR [29,30]. The wear coefficient tends to a constant value as the sliding distance increases, as shown in Figure 8(a), while the volume of removed material (VRM) has a linear relation with the test duration in the SSR, please see Figure 8(b). The deviation observed before the SSR is due to the difficulty to measure the wear crater in the early stages of the test.

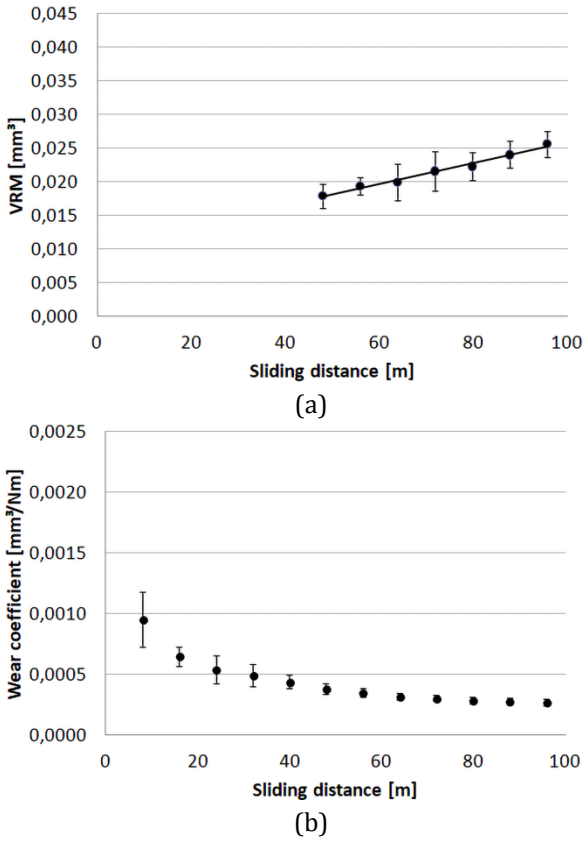

Fig. 8. Test evolution in a Zn + nano-coating specimen at a normal load of 0.98 N and a slurry concentration of 0.244 g/cm^3. (a) k = f(S); (b)VRM = f(S).

Due to the fact that the SSR is achieved when the variation of the VMR as a function of the sliding distance shows linear behavior, and R^2 values near the unit were obtained, it can be assumed that the SSR was really achieved for all tested conditions. Table 2 summarizes the obtained values of the wear coefficient (k) and the linear regression coefficient (R^2) for all tested conditions. The mean wear coefficient values shown in Table 2 do not consider the values before the SSR.

Table 2. Wear coefficients (k) and linear regression coefficients (R2) for all tested conditions.

Condition	Load [N]	Slurry Conc. [g/cm^3]	k [mm^3/Nm]	R^2
Zn + nano-coating	0.49	0.244	3.86E-04	0.97
Zn + nano-coating	0.98	0.244	2.92E-04	0.97
Zn + nano-coating	0.49	0.733	6.48E-04	0.98
Zn + nano-coating	0.98	0.733	4.44E-04	0.99
Zn-coating	0.49	0.244	4.67E-04	0.99
Zn-coating	0.98	0.244	2.45E-04	0.98
Zn-coating	0.49	0.733	6.45E-04	0.99
Zn-coating	0.98	0.733	4.44E-04	0.98

According to Table 2, when the wear coefficient results are compared between Zn-coating and Zn + nano-coating conditions, for the same applied load and slurry abrasive concentration, there is no significant change in the wear coefficient. Thus, the nanoceramic coating seems to have no influence on the wear resistance for the conditions tested in this work. As observed in Figure 5 (c) and (d), the nano-coating adhesion to the Zn underlayer for Zn + nano-coating samples is insufficient, resulting in a completely detachment of the SiO_2 layer. As consequence, the wear resistance between Zn-coating and Zn + nano-coating samples are very similar due to the decrease in the load bearing capacity [31,32].

For a direct comparison between the Zn + nano-coating samples, it is noticed that an increase in the applied load leads to a reduction in the wear coefficient of 24% and 31% for abrasive slurry concentrations of 0.244 g/cm^3 and 0.733 g/cm^3, respectively. A similar behavior occurs for the Zn-coating samples, where the same increase in the applied load leads to a reduction in the wear coefficient of 48% and 31% for abrasive slurry concentrations of 0.244 g/cm^3 and 0.733 g/cm^3, respectively. This behavior is due the fact that, when the load increases, fewer abrasive particles enter in the ball-sample contact region, thus reducing the wear coefficient [12,33].

In turn, when the abrasive slurry concentration increases, an increase of 60% and 52% is observed in the wear coefficient for applied loads of 0.49 N and 0.98 N, respectively, for the Zn + nano-coating samples. For the Zn-coating samples

the increase in the wear coefficient is 38% and 81% for applied loads of 0.49 N and 0.98 N, respectively. As the abrasive slurry concentration increases, more particles enter the contact region. As these particles are larger (80% are between 1μm and 5 μm) than the thickness of the SiO2 layer (Zn + nano-coating samples), in greater contractions the layer delamination is facilitated. For thicker layers, abrasive particles would not be able to penetrate the layer to the point of causing delamination and consequent acceleration of the wear process, especially in the initial moments of the test [34].

Figures 9 and 10 shows the wear craters of Zn-coating and Zn + nano-coating, respectively, for an applied load of 0.98 N and an abrasive slurry concentration of 0.733 g/cm^3.

Once the presence of Fe atoms - Figures 9(c) and 10(c) - is detected, it is possible to state that the AISI 1020 steel substrate is exposed during the wear process. Furthermore, there is no presence of Zn atoms inside the wear craters, as observed in Figures 9(d) and 10(d). Thus, it can be stated that both the zinc layer and the nanoceramic coating are completely removed after a sliding distance of approximately 100 meters.

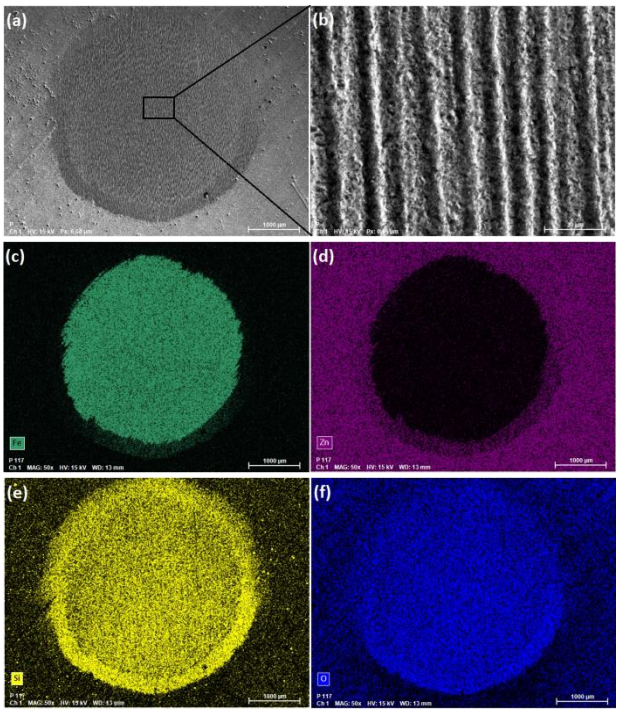

Fig. 9. (a) Wear crater of Zn-coating sample abraded at 0.98 N and 0.733 g/cm^3 (a); (b) higher magnification of the rectangle showed in (a); (c)-(f) EDS mapping of Fe, Zn, Si and O, respectively.

In Figure 9(e) and (f) the presence of Si and O atoms, respectively is attributed to the embedment of SiO_2 abrasive particles from the slurry since it seems to be a greater concentration of these elements inside the wear crater than outside. In ductile materials, the attachment of abrasive particles results in the decrease of the abrasive wear coefficient [35,36].

Otherwise, in Figure 10(e) and (f), the presence of Si and O atoms outside the wear crater is related to the SiO_2 coating layer formed during the nanoceramic coating process and is in good agreement with the XRD results showed previously. The SiO_2 layer is delaminated even in regions outside the wear crater.

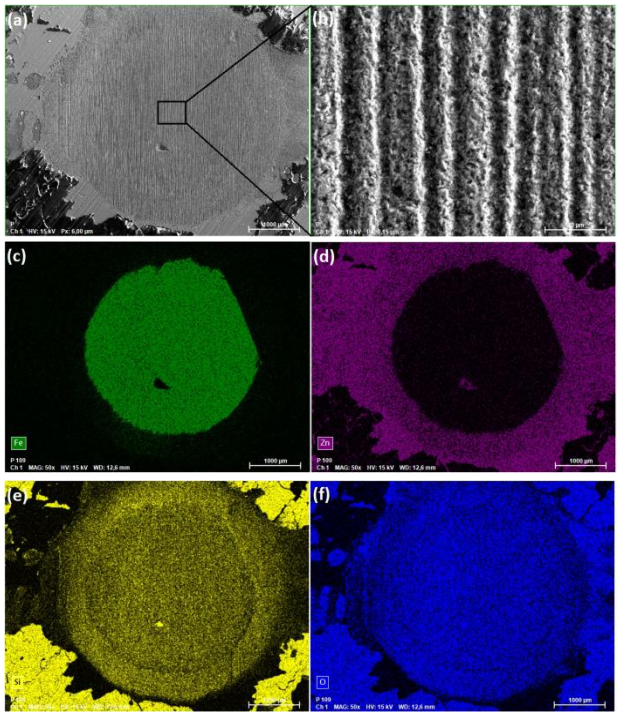

Fig. 10. (a) Wear crater of Zn + nano-coating sample abraded at 0.98 N and 0.733 g/cm^3 (a); (b) higher magnification of the rectangle showed in (a); (c)-(f) EDS mapping of Fe, Zn, Si and O, respectively.

In Figures 9(b) and 10(b) a higher magnification of the rectangles showed in Figures 9(a) and 10(a) is presented. As can be noted, the main wear mechanism observed was grooving abrasion due to the presence of grooves in the sliding wear direction (upright). Despite this fact, some indentations marks are also observed along the grooves.

The occurrence of grooving or rolling abrasion in micro-scale abrasive wear tests is closely related to the sliding distance. Usually, due to the fact that the tests are conducted with constant applied load, the decrease in contact pressure and, consequently, the severity of the test, there is a variation in the wear mechanisms [11] with a tendency to occur rolling abrasion [37]. Despite the abrasive slurry concentration being kept constant during the test, with the decrease in contact pressure due to the increase in the projected area of the wear crater, there is a decrease in the load per abrasive particle with the increase in the sliding distance [15,38]. The decrease in the load per abrasive particle then favors the occurrence of the rolling-abrasion mechanism [39]. Therefore, the wear mechanism observed in this work can be described as grooving-abrasion with the tendency of occurring rolling-abrasion for longer sliding distances.

4. CONCLUSIONS

Microstructural analysis, evaluation of layer adhesion, corrosion resistance and micro-scale abrasive wear test were carried out in order to evaluate the performance of a comercial nanoceramic sealant deposited on galvanized AISI 1020 steel. After the tests, the following conclusions can be drawn:

- The nanoceramic sealant adhesion to the substrate failed the adhesion test within the established conditions and is prone to suffer significant micro-cracking and/or delamination;
- The corrosion rate of the Zn + nano-coating sample reduced by 62.2% when compared to the Zn-coating sample;
- There is no significant change in the wear coefficient between Zn-coating and Zn + nano-coating samples for the same micro-scale abrasive wear conditions;
- Independent of the sample condition, an increase in the applied load resulted in decrease of the wear coefficient, while an increase in the abrasive slurry concentration, increases the wear coefficient;
- The wear mechanism observed is grooving-abrasion with the tendency of occurring rolling-abrasion for longer sliding distances.

It is important to carry out tests applying corrections to the deposition parameters in order to guarantee adhesion and a greater layer thickness. Therefore, a direct comparison with the results presented in this work will help to understand the problems and probably align the processes to justify the use of the studied coating. One option is to change the base coating of the current galvanization to zinc-iron as it has greater mechanical resistance.

Acknowledgement

The authors would like to acknowledge the IFSC, UDESC and UniSENAI for the infrastructure made available for carrying out this work.

REFERENCES

[1] E. Almeida, “Surface treatments and coatings for metals. A General Overview. 1. Surface treatments, surface preparation, and the nature of coatings,” *Industrial & Engineering Chemistry Research*, vol. 40, no. 1, pp. 3–14, Dec. 2000, doi: 10.1021/ie000209l.

[2] A. Ghanbari and M. M. Attar, “Surface free energy characterization and adhesion performance of mild steel treated based on zirconium conversion coating: A comparative study,” *Surface & Coatings Technology*, vol. 246, pp. 26–33, May 2014, doi: 10.1016/j.surfcoat.2014.02.057.

[3] I. Milošev and G. S. Frankel, “Review-Conversion coatings based on zirconium and/or titanium,” *Journal of the Electrochemical Society*, vol. 165, no. 3, pp. 127–44, Jan. 2018, doi: 10.1149/2.0371803jes.

[4] Y.T. Chang, N.-T. Wen, W.K. Chen, M.D. Ger, G.T. Pan, and T. C. K. Yang, “The effects of immersion time on morphology and electrochemical properties of the Cr(III)-based conversion coatings on zinc coated steel surface,” *Corrosion Science*, vol. 50, no. 12, pp. 3494–3499, Dec. 2008, doi: 10.1016/j.corsci.2008.08.051.

[5] A. Ghanbari, M. M. Attar, and M. Mahdavian, “Corrosion inhibition performance of three imidazole derivatives on mild steel in 1M phosphoric acid,” *Materials Chemistry and Physics*, vol. 124, no. 2–3, pp. 1205–1209, Dec. 2010, doi: 10.1016/j.matchemphys.2010.08.058.

[6] Q. Liu *et al.*, “Corrosion resistance and adhesion behavior of an octa-(aminopropyl) polyhedral oligomeric silsesquioxane-modified graphene oxide-incorporated conversion coating for hot-dip galvanized steel,” *Surface & Coatings Technology*, vol. 409, p. 126900, Mar. 2021, doi: 10.1016/j.surfcoat.2021.126900.

[7] D. Mikičić, A. Kunosić, M. Zlatanović, "Contact force determination in abrasive wear test," *Tribology in Industry*, vol. 27, no. 1-2, pp. 34–37, 2005.

[8] K. Adachi and I. Hutchings, "Wear-mode mapping for the micro-scale abrasion test," *Wear*, vol. 255, no. 1–6, pp. 23–29, Aug. 2003, doi: 10.1016/s0043-1648(03)00073-5.

[9] A. C. Bozzi, F. D. Ramos, and D. B. O. Vargas, "Microabrasive wear behavior of different stellites obtained by laser cladding and casting processes," *Wear*, vol. 524–525, p. 204857, Jul. 2023, doi: 10.1016/j.wear.2023.204857.

[10] K. L. Rutherford and I. M. Hutchings, "A micro-abrasive wear test, with particular application to coated systems," *Surface & Coatings Technology*, vol. 79, no. 1–3, pp. 231–239, Feb. 1996, doi: 10.1016/0257-8972(95)02461-1.

[11] K. Schiffmann, R. Bethke, and N. Kristen, "Analysis of perforating and non-perforating micro-scale abrasion tests on coated substrates," *Surface & Coatings Technology*, vol. 200, no. 7, pp. 2348–2357, Dec. 2005, doi: 10.1016/j.surfcoat.2005.01.015.

[12] M. G. Gee *et al.*, "Progress towards standardisation of ball cratering," *Wear*, vol. 255, no. 1–6, pp. 1–13, Aug. 2003, doi: 10.1016/s0043-1648(03)00091-7.

[13] Y. Kusano, K. Van Acker, and I. Hutchings, "Methods of data analysis for the micro-scale abrasion test on coated substrates," *Surface & Coatings Technology*, vol. 183, no. 2–3, pp. 312–327, May 2004, doi: 10.1016/j.surfcoat.2003.10.010.

[14] D.N. Allsopp, R.I. Trezona, I.M. Hutchings, "The effects of ball surface condition in the micro-scale abrasive wear test," *Tribology Letters*, vol. 5, pp. 259–264, Nov. 1998, doi:10.1023/A:1019178716408.

[15] R. I. Trezona, D. N. Allsopp, and I. Hutchings, "Transitions between two-body and three-body abrasive wear: influence of test conditions in the microscale abrasive wear test," *Wear*, vol. 225–229, pp. 205–214, Apr. 1999, doi: 10.1016/s0043-1648(98)00358-5.

[16] P. S. Martins, S. S. Pires, E. R. Da Silva, V. F. Vieira, E. C. T. Ba, and C. Dias, "Tribological aspects of the Diamond-like carbon film applied to different surfaces of AISI M2 steel," *Wear*, vol. 506–507, p. 204469, Oct. 2022, doi: 10.1016/j.wear.2022.204469.

[17] A. J. Gant and M. G. Gee, "A review of micro-scale abrasion testing," *Journal of Physics D: Applied Physics*, vol. 44, no. 7, p. 073001, Jan. 2011, doi: 10.1088/0022-3727/44/7/073001.

[18] M.S. Priyan, P. Hariharan, "Abrasive wear modes in ball-cratering test conducted on $Fe_{73}Si_{15}$ $Ni_{10}Cr_2$ alloy deposited specimen," *Tribology in Industry*, vol. 36, no. 1, pp. 97–106. Mar. 2014.

[19] N. Vidakis, A. Antoniadis, and N. Bilalis, "The VDI 3198 indentation test evaluation of a reliable qualitative control for layered compounds," *Journal of Materials Processing Technology*, vol. 143–144, pp. 481–485, Dec. 2003, doi: 10.1016/s0924-0136(03)00300-5.

[20] J. Xu, S. Peng, Z. Li, S. Jiang, Z. Xie, and P. Munroe, "The influence of semiconducting properties of passive films on the cavitation erosion resistance of a NbN nanoceramic coating," *Ultrasonics Sonochemistry*, vol. 71, p. 105406, Mar. 2021, doi: 10.1016/j.ultsonch.2020.105406.

[21] H. Wu *et al.*, "A wear-resistant TiO_2 nanoceramic coating on titanium implants for visible-light photocatalytic removal of organic residues," *Acta Biomaterialia*, vol. 97, pp. 597–607, Oct. 2019, doi: 10.1016/j.actbio.2019.08.009.

[22] Ş. Taktak and S. Taşgetiren, "Identification of delamination failure of boride layer on common CR-Based steels," *Journal of Materials Engineering and Performance*, vol. 15, no. 5, pp. 570–574, Oct. 2006, doi: 10.1361/105994906x124587.

[23] L. I. Farfán-Cabrera, C. D. Resendiz-Calderon, A. Hernandez-Peña, I. Campos-Silva, E. A. Gallardo-Hernández, and A. D. Contla-Pacheco, "Tribological effects of boriding treatment on a low carbon steel repaired by wire and arc additive manufacturing," *Surface & Coatings Technology*, vol. 465, p. 129574, Jul. 2023, doi: 10.1016/j.surfcoat.2023.129574.

[24] L. Xiao *et al.*, "Study on corrosion mechanism of Al–Zn coatings in the simulated polluted marine atmosphere," *Journal of Materials Research and Technology*, vol. 25, pp. 6446–6458, Jul. 2023, doi: 10.1016/j.jmrt.2023.07.091.

[25] E. McCafferty, "Validation of corrosion rates measured by the Tafel extrapolation method," *Corrosion Science*, vol. 47, no. 12, pp. 3202–3215, Dec. 2005, doi: 10.1016/j.corsci.2005.05.046.

[26] S. Wang *et al.*, "Study of the corrosion behavior and mechanism of a hot-dipping Zn–6Al–3Mg alloy coating in 3.5 wt% neutral NaCl solution," *Surface & Coatings Technology*, vol. 464, p. 129576, Jul. 2023, doi: 10.1016/j.surfcoat.2023.129576.

[27] A. P. Krelling, F. Teixeira, C. E. Da Costa, E. A. D. S. De Almeida, B. F. Zappelino, and J. C. G. Milan, "Microabrasive wear behavior of borided steel abraded by SiO_2 particles," *Journal of Materials Research and Technology*, vol. 8, no. 1, pp. 766–776, Jan. 2019, doi: 10.1016/j.jmrt.2018.06.004.

[28] A. P. Krelling, E. A. D. S. De Almeida, C. E. Da Costa, and J. C. G. Milan, "Microstructural and tribological characterization of niobium boride coating produced on AISI 1020 steel via multicomponent boriding," *Materials Research Express*, vol. 7, no. 2, p. 026413, Feb. 2020, doi: 10.1088/2053-1591/ab7266.

[29] E. A. D. S. De Almeida *et al.*, "Micro-abrasive wear behavior of nitrided and multilayer coated high vanadium powder metallurgy alloy," *Metallurgical and Materials Transactions*, vol. 51, no. 3, pp. 1334–1344, Jan. 2020, doi: 10.1007/s11661-019-05621-2.

[30] W. M. Da Silva, M. P. Suarez, Á. R. Machado, and H. L. Costa, "Effect of laser surface modification on the micro-abrasive wear resistance of coated cemented carbide tools," *Wear*, vol. 302, no. 1–2, pp. 1230–1240, Apr. 2013, doi: 10.1016/j.wear.2013.01.035.

[31] J. C. A. Batista, C. Godoy, V. T. L. Buono, and A. Matthews, "Characterisation of duplex and non-duplex (Ti, Al)N and Cr–N PVD coatings," *Materials Science and Engineering: A*, vol. 336, no. 1–2, pp. 39–51, Oct. 2002, doi: 10.1016/s0921-5093(01)01953-0.

[32] F. Hakami, M. H. Sohi, and J. R. Ghani, "Duplex surface treatment of AISI 1045 steel via plasma nitriding of chromized layer," *Thin Solid Films*, vol. 519, no. 20, pp. 6792–6796, Aug. 2011, doi: 10.1016/j.tsf.2011.04.054.

[33] P. J. Esteves, V. Seriacopi, M. C. S. De Macêdo, R. M. Souza, and C. Scandian, "Combined effect of abrasive particle size distribution and ball material on the wear coefficient in micro-scale abrasive wear tests," *Wear*, vol. 476, p. 203639, Jul. 2021, doi: 10.1016/j.wear.2021.203639.

[34] J. C. A. Batista, C. Godoy, and A. Matthews, "Micro-scale abrasive wear testing of duplex and non-duplex (single-layered) PVD (Ti, Al)N, TiN and Cr–N coatings," *Tribology International*, vol. 35, no. 6, pp. 363–372, Jun. 2002, doi: 10.1016/s0301-679x(02)00017-8.

[35] J. O. Bello and R. J. K. Wood, "Grooving micro-abrasion of polyamide 11 coated carbon steel tubulars for downhole application," *Wear*, vol. 255, no. 7–12, pp. 1157–1167, Aug. 2003, doi: 10.1016/s0043-1648(03)00226-6.

[36] K. Bose and R. J. K. Wood, "Influence of load and speed on rolling micro-abrasion of CVD diamond and other hard coatings," *Diamond and Related Materials*, vol. 12, no. 3–7, pp. 753–756, Mar. 2003, doi: 10.1016/s0925-9635(02)00238-8.

[37] G. H. S. Gava, R. M. Souza, J. D. B. De Mello, M. C. S. De Macêdo, and C. Scandian, "Effect of load partition and particle distribution on micro-abrasive wear mapping of two-phase metal matrix composites," *Wear*, vol. 301, no. 1–2, pp. 130–136, Apr. 2013, doi: 10.1016/j.wear.2012.11.080.

[38] M. Stack and M. T. Mathew, "Micro-abrasion transitions of metallic materials," *Wear*, vol. 255, no. 1–6, pp. 14–22, Aug. 2003, doi: 10.1016/s0043-1648(03)00204-7.

[39] R. C. Cozza, "Effect of sliding distance on abrasive wear modes transition," *Journal of Materials Research and Technology*, vol. 4, no. 2, pp. 144–150, Apr. 2015, doi: 10.1016/j.jmrt.2014.10.007.